In-Depth Insights into the Key Steps of Delamination of Charged 2D Nanomaterials
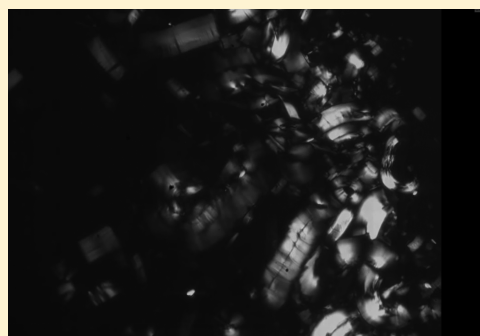
Sabine Rosenfeldt,[†] Matthias Stöter,[‡] Mathias Schlenk,[†] Thomas Martin,[‡] Rodrigo Queiroz Albuquerque,[∥,§] Stephan Förster,*[,†] and Josef Breu*[,‡]

[†]Physical Chemistry I and [‡]Inorganic Chemistry I, University of Bayreuth, Universitätsstrasse 30, 95440 Bayreuth, Germany
[§]São Carlos Institute of Chemistry, University of São Paulo, Av. Trab. Sao-carlense 400, 13560-970 São Carlos, Brazil

Ⓢ Supporting Information

ABSTRACT: Delamination is a key step to obtain individual layers from inorganic layered materials needed for fundamental studies and applications. For layered van der Waals materials such as graphene, the adhesion forces are small, allowing for mechanical exfoliation, whereas for ionic layered materials such as layered silicates, the energy to separate adjacent layers is considerably higher. Quite counterintuitively, we show for a synthetic layered silicate ($Na_{0.5}$-hectorite) that a scalable and quantitative delamination by simple hydration is possible for high and homogeneous charge density, even for aspect ratios as large as 20000. A general requirement is the separation of adjacent layers by solvation to a distance where layer interactions become repulsive (Gouy–Chapman length). Further hydration up to 34 nm leads to the formation of a highly ordered lamellar liquid crystalline phase (Wigner crystal). Up to eight higher-order reflections indicate excellent positional order of individual layers. The Wigner crystal melts when the interlayer separation reaches the Debye length, where electrostatic interactions between adjacent layers are screened. The layers become weakly charge-correlated. This is indicated by fulfilling the classical Hansen-Verlet and Lindeman criteria for melting. We provide insight into the requirements for layer separation and controlling the layer distances for a broad range of materials and outline an important pathway for the integration of layers into devices for advanced applications.

INTRODUCTION

Two-dimensional (2D) materials have an atomic organization where the bond strengths along two dimensions are much stronger compared to the third dimension.[1] The crystal structures typically consist of thin layers of atoms with strong directional bonding within the layers and much weaker interactions between the layers. If the layers are neutral, they form van der Waals solids with only weak layer interaction. Prominent examples for these materials are graphene and transition metal dichalcogenides such as MoS_2, WS_2, or WSe_2. For charged layers such as in layered silicates, the layer interactions are much stronger. Exfoliated or delaminated nanosheets of 2D-materials have unusual phononic,[2] electronic,[3,4] ferroic,[5] electrochemical,[6] and mechanical properties[7,8] which are used in phononics, photovoltaics, semiconductors, and electrodes. Those properties are strongly tied to the limitation or annihilation of translational symmetry along the stacking direction. When individual monolayers are homogeneously dispersed in a matrix, the related composite materials have a maximized, huge surface-to-volume ratio, and for large aspect ratios (ratio of diameter to layer thickness), these materials process a very small percolation threshold to provide electrical and thermal conductivity, mechanical strength, and large tortuous paths for diffusion barriers. Therefore, control over the layer thickness and interlayer distance is essential. For van der Waals solids, the weak

interlayer interaction energies (4–7 kJ/mol) can be overcome by mechanical forces (mechanical exfoliation). A simple and prominent case is the exfoliation of graphene layers using "Scotch tape".[9] The "Scotch tape" method is, however, limited to fundamental research in small scale. Various other techniques ranging from epitaxial growth to mechanical exfoliation, potentially assisted by surface active compounds or by rendering the starting material more shear labile by intercalation reactions, have been shown to yield 2D materials. Established techniques, however, tend to produce broad distributions of layers[5,10−12] because separation by mechanical exfoliation is incomplete and, moreover, usually comes along with breakage of the layers.

The same conclusions are valid for the exfoliation of ionic layers, where the exfoliation process is even more difficult due to the stronger attractive interactions between the layers, which are of the order of 100 kJ/mol and larger. Separation procedures almost exclusively rely on mechanical exfoliation with the aid of intercalation of large ions, molecules, or surface-active compounds, albeit with generally poor and incomplete exfoliation. Even in the case of high shear rates, the aspect ratio never reaches its intrinsic maximum defined by the pristine
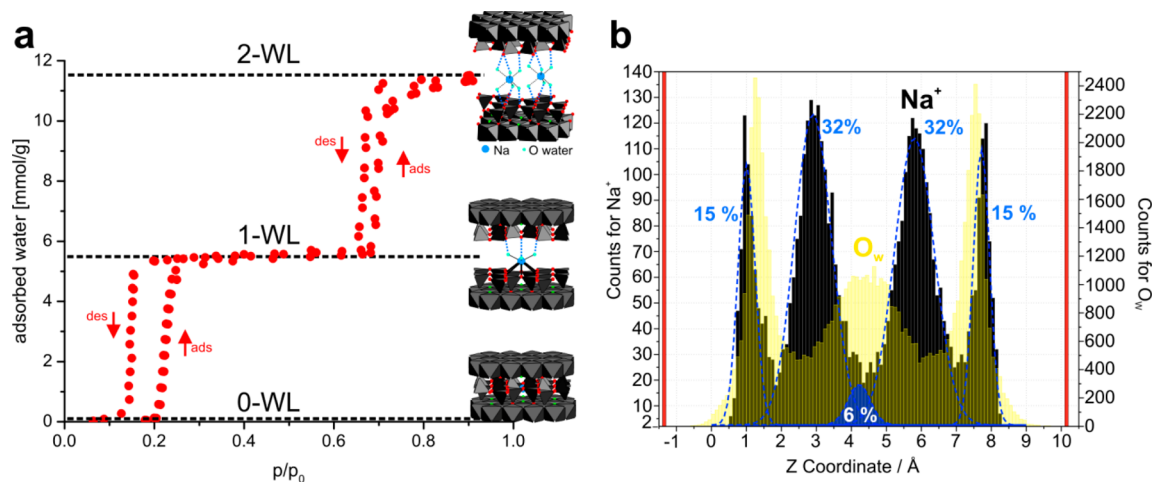
Figure 1. (a) Water vapor sorption isotherm of $Na_{0.5}$-hectorite and corresponding hydrated structures of 0-, 1-, and 2-WL hydrates. (b) Histogram of the Z-distribution of Na^+ (black bars) and oxygens ("O_w", yellow bars) of water molecules in the interlayer space of the hectorite obtained during 1 ns of MD simulation (NVT, 300 K). Red bars represent the plane of basal oxygens of the tetrahedral layers. The five blue gaussians are the deconvoluted peaks of the black bars.

lateral extension of the inorganic stacks. Alternatively, osmotic swelling potentially represents a gentler, inexpensive,and scalable route to utterly separate a layered material into singular layers.

The principle of osmotic swelling goes back to the swelling of graphite oxide (1932)[13] and montmorillonite.[14] Here we report a systematic study of the exfoliation of a synthetic 2D layered silicate via osmotic swelling that provides direct insight into the conditions for ionic layer separation and the buildup of the electric double layer and outlines the lyotropic phase behavior at extreme aspect ratios of the resulting layered material over more than 4 orders of magnitude at concentrations from the dry powder to highly dilute solutions.

■ RESULTS AND DISCUSSIONS

Osmotic delamination is known empirically to require a well-defined homoionic layered material with high and very homogeneous charge density. Natural layered silicates suffer from pronounced charge density modulations at all length scales.[15] Even synthetic layered silicates when synthesized at temperatures below 1000 K show a nonuniform intracrystalline reactivity. As a consequence, a large fraction of the stacks does not show osmotic swelling at all, or the separation between adjacent layers varies randomly and a weighted average of the d-spacings is observed which is of limited analytical and practical value.[16] Moreover, all the above-mentioned materials need to be ion-exchanged and/or purified in some way prior to osmotic swelling. For instance, for montmorillonite a selective dissolution of amorphous auxiliary minerals such as iron oxyhydroxides is applied, where concomitantly ion exchange occurs and homoionic Na-montmorillonite is obtained.[17] Following purification, the ionic strength needs to be reduced and finally the suspensions need to be reconcentrated physically, e.g., by sedimentation or centrifugation, to solid contents where liquid crystalline (LC) phases are observed. For kinetic reasons during the concentration procedure, equilibrium structures might not be readily achieved.[18]

Here we use a synthetic hectorite with a composition in the unit cell of $[Na_{0.96}]^{inter}[Mg_{5.14}Li_{0.94}]^{oct}[Si_8]O_{20}F_4$ (two formula units per unit cell and therefore abbreviated as $Na_{0.5}$-hectorite) that has been synthesized from the melt at temperatures well

above 1000 K.[19] The material does not require any purification and shows a very homogeneous intracrystalline reactivity. With this material at hand, delamination and swelling can be studied starting with a 1D crystalline dry powder all the way into the LC regime and beyond simply by adding increasing amounts of water.

Regime I: Crystalline Swelling (Attractive). The first steps of layer separation occur via discrete hydration steps as indicated by the adsorption isotherm (Figure 1a) of synthetic $Na_{0.5}$-hectorite.[19] The transitions from nonhydrated (0-WL) to the first water layer (1-WL) and the second water layer (2-WL) occur at threshold partial pressures of $p/p_0 = 0.22$ and $p/p_0 = 0.64$, respectively. The observed hysteresis indicates that the phase transitions are first-order, which is also suggested by MD-simulations.[26−28] All structures consist of equidistant layers with long-range 1D ordering within a stack which is referred to as a tactoid. Adjacent layers are stacked in an uncorrelated mode (turbostratic stacking). For more highly charged layered silicates, in some rare cases three-dimensionally ordered phases can be obtained making crystal structure solutions of 1-WL and 2-WL hydrates available.[20,21]

In the 1-WL state an inner sphere Na-hydrate complex is observed where Na^+ is in direct contact with basal oxygen atoms on one side, due to Coulomb attraction, and is coordinated by three water molecules on the other side. In the 2-WL state, an outer sphere hexaaquo-Na^+-complex occupies the middle of the interlayer space with symmetrical hydrogen bonding to both adjacent basal oxygen planes.[20]

For the more highly charged synthetic hectorite, the 3-WL structure is not accessible within the experimentally accessible humidity range. It has been observed for natural montmorillonites of lower charge density, i.e., $\sigma_s = 0.66$ charges per nm^2, where the hexaaquo-Na^+-complexes were found to predominantly stay in close contact with only one of the silicate layer surfaces.[22] To verify this configuration for the synthetic Na^+-hectorite, we performed MD-simulations of the 3-WL structure. Details of the calculations are given in the Supporting Information. We found that 30% of the Na^+-cations were coordinated to the basal oxygens and formed an inner-sphere complex, similar to that in the 1-WL structure, and 64% formed hexaaquo-Na^+-cations located at distances of 0.24 Å away from

the surface, similar to that in the 2-WL structure. Additionally, 6% formed a hexaaquo-Na$^+$-complex in the center of the interlayer space. Upon increasing hydration (0-WL → 1-WL → 2-WL → 3-WL), we observe a structural evolution from surface associated nonhydrated via partially and fully hydrated counterions to finally surface detached counterions. In the 3-WL phase the surface-separated counterions start localizing in the midplane between the two surfaces. This represents the buildup of the classical counterion double layer structure (Grahame model) with a sequence of three layers: (a) The first layer is the inner Helmholtz plane, where the counterions are located at the charged surface, (b) followed by an outer Helmholtz plane with surface-separated, fully hydrated ions, and (c) a diffusive double layer with nonlocalized ions at the midplane (where the electric field vanishes). A full development of the diffuse double layer would eventually lead to electrostatic repulsion,[22,23] driving the separation of adjacent layers.

Transition I: Crystalline to Osmotic Swelling. To obtain insight into the conditions for separation of charged layers, as a first approximation the relevant interaction energies and length scales are estimated from simple physical models:

(a) For ion−ion interactions, the important length scale is the Bijerrum length:

$$l_B = \frac{e^2}{4\pi\varepsilon\varepsilon_0 k_B T} \tag{1}$$

which is the distance at which Coulomb interactions between ions are equal to the thermal energy $k_B T$. e is the elementary charge, ε_0 the vacuum permittivity, and ε the dielectric constant. Taking water ($\varepsilon = 78$) at $T = 298.15$ K (25 °C), the Bijerrum length is equal to $l_B = 0.71$ nm.

(b) For ion−surface interactions, the relevant length scale is the Gouy−Chapman length:

$$l_{GC} = \frac{1}{2\pi l_B \sigma_s} \tag{2}$$

the distance of an ion to a charged surface where electrostatic surface−ion interactions are equal to the thermal energy. σ_s is the surface charge density (in units of $1/m^2$). For a charge density of 1 charge per nm^2 (0.96 charges per $2(a \times b) = 0.95$ nm), as in the present system, the Gouy−Chapman length $l_{GC} = 0.22$ nm.

(c) As a measure of the degree of electrostatic coupling of the ions to the surface, one defines a coupling parameter:[24]

$$\Xi = \frac{l_B}{l_{GC}} \tag{3}$$

where in case of $\Xi \gg 1$ the counterions are strongly coupled to the surface. For the present case, we have $\Xi = 3.2$ such that the surface-coupling of counterions is significant.

(d) The Debye length for the case of monovalent ions is given by

$$\kappa^{-1} = \left(\frac{\varepsilon\varepsilon_0 k_B T}{2 N_A e^2 c_I}\right)^{1/2} \tag{4}$$

and is the length scale beyond which electrostatic interactions are screened. If no specific measures are taken to remove ionic impurities from aqueous solutions, one has a typical ion concentration of $c_I = 10^{-4}$ mol/L which corresponds to a Debye length of $\kappa^{-1} = 30$ nm.

These electrostatic length scales will be related to the layer surface separation h to distinguish different regimes with characteristic properties. The onset of repulsion of adjacent silicate layers is related to the trade-off between short-range attractive electrostatic interactions, hydration forces, and counterion translational entropy. For small h on the order of the Gouy−Chapman length ($h \approx l_{GC}$, regime I), we have a competition between attractive surface−counterion interactions with an energy $F_{el} \approx - h k_B T / l_{GC}$ and a repulsive entropic contribution due to the translational entropy of the counterions, given by $F_S \approx k_B T \ln h$, which increases with increasing layer surface separation h. Both contributions result in an osmotic pressure between the surfaces given by[24]

$$\Pi = \sigma_s \frac{\partial F}{\partial d} \approx l_{GC} \sigma_s k_B T \left(\frac{2 l_{GC}}{h} - 1\right) \tag{5}$$

For layer surface separation $h > 2 l_{GC} = 0.44$ nm according to this simple model, repulsive interactions are expected.

For layered silicates, the initial separation during crystalline swelling is driven by the strong hydration forces, which for Na$^+$ involve an energy of 406 kJ/mol. With the silicate layer thickness of 0.96 nm as determined by the interlayer distance of nonhydrated Na$_{0.5}$-hectorite,[19] the 2-WL structure would already be expected to be in the repulsive regime ($h \approx 1.55 - 0.96$ nm = 0.59 nm > $2 l_{GC}$). Experimentally, 2-WL is found to be still stabilized at a discrete hydration state. Yet, the value of 0.59 nm is not significantly larger than the estimated threshold of 0.44 nm, as secondary attractive interactions such as lateral or specific ion or solvent correlations, van der Waals interactions, and hydrogen bonding were neglected. For the 3-WL structure, $h \approx 1.83 - 0.96$ nm = 0.87 nm, the repulsive regime is finally entered. The interactions applied in the MD simulation are more realistic and correctly indicated the transition to the repulsive regime with the 3-WL structure. The calculations predict that layer charge variations or inhomogeneities, which directly affect l_{GC}, may easily lead to a situation where domains with repulsive and attractive interactions coexist within a layer. Even when there is a small fraction of the latter, it will prevent the separation of adjacent layers by osmotic swelling. This problem becomes increasingly severe with increasing lateral diameter of the tactoids relevant for practical applications.

Regime II: Osmotic Swelling in the Gouy−Chapman Regime. After the attractive short-range surface−ion interactions have been overcome by hydration such that $h \gg 2 l_{GC}$, repulsive interactions between the layers dominate. Further addition of water will then lead to a continuous further separation of the layers. This regime is characterized by the length scales $l_D \gg h \gg l_{GC}$. This regime is referred to as the Gouy−Chapman regime. Here the osmotic pressure between adjacent layers separated by a distance h is given by[24]

$$\Pi \approx \frac{\pi k_B T}{2 l_B} \frac{1}{h^2} \tag{6}$$

and thus becomes independent of the surface charge density σ_s and the related ion−surface interactions. The osmotic pressure is now dominated by ion−ion interactions characterized by the Bijerrum length l_B and is quite long-ranged, i.e., proportional to h^{-2}.

As suggested by this model, with addition of water the layers completely separate and the silicate/water mixture forms transparent gels. Gel formation was noticed as early as the
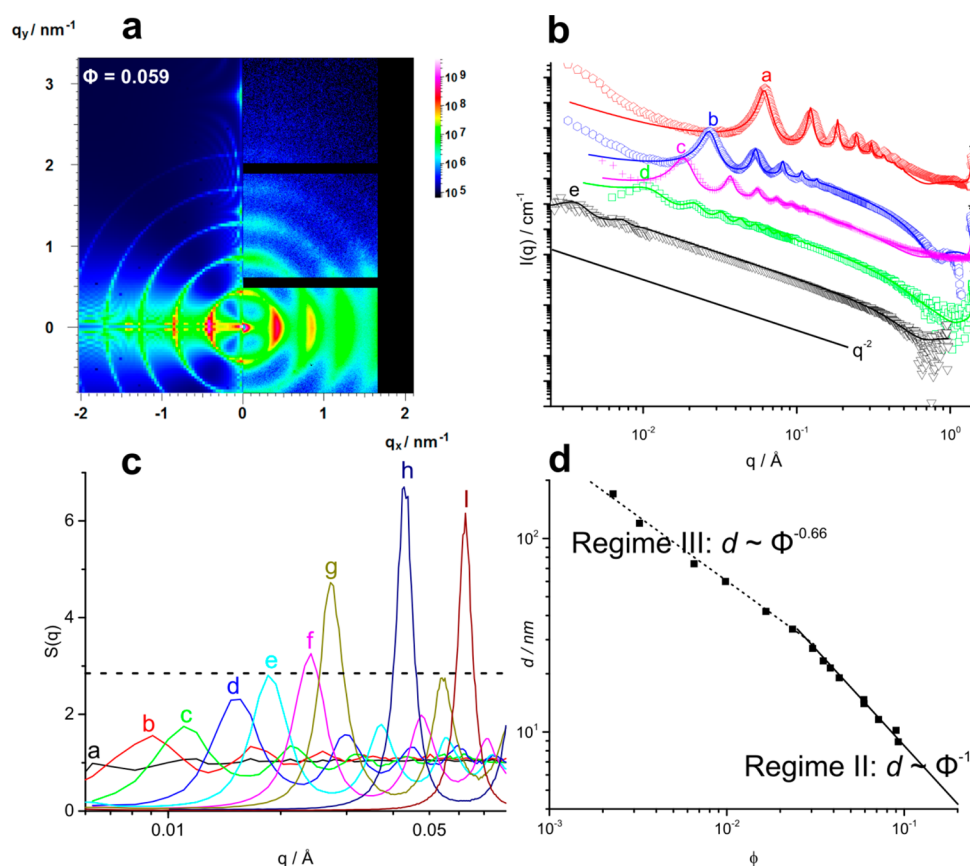
Figure 2. (a) 2D-SAXS pattern at volume fraction ϕ = 0.059. On the right side, experimental data are plotted, and on the left side modeled patterns are shown. (b) The one-dimensional (1D) SAXS intensity shows a shift of the 001 reflection to higher d-spacings with decreasing concentration and the concentration-independent position of the hk-band (asterisk) at high q. (a: ϕ = 0.090 (red pentagons); b: ϕ = 0.035 (blue hexagons); c: ϕ = 0.024 (magenta crosses), d: ϕ = 0.010 (green squares); e: ϕ = 0.0016 (black triangles). Calculated scattering curves and the q^{-2}-scaling law of layers are given by solid lines. (c) Structure factor of swollen lyotropic phases at different volume fractions. (a) ϕ = 0.003; (b) ϕ = 0.007; (c) ϕ = 0.010, (d) ϕ = 0.017, (e) ϕ = 0.024, (f) ϕ = 0.030; (g) ϕ = 0.035; (h) ϕ = 0.059; (i) ϕ = 0.090. The dashed line at $S(q)$ = 2.85 marks the Hansen-Verlet rule where melting is expected. (d) Scaling relation d-spacing as a function of volume fraction. The solid line corresponds to a 1D-swelling law following the equation $d = D/\phi$, which fits both crystalline swelling and Wigner crystal regime. The gradient in the nematic sol regime (dashed line) follows a distinct scaling ($d \sim \phi^{-0.66}$).

1930s and at that time was related to the "house-of-cards" model, a connected network of edge-basal plane interactions of layers.[23] An alternative interpretation of the gel phase was proposed by Langmuir in 1938 who described it as a lamellar lyotropic phase.[25] This was later confirmed by Michot and Miyamoto (2006) for a series of layered silicates including nontronite, montmorillointe,[26−28] beidellite,[29] laponite,[18] fluorotetrasilicic mica,[30] and fluorohectorite.[30,31] Lamellar lyotropic phases were also found by Gabriel et al. in 2001 for a solid acid, $H_3Sb_3P_2O_{14}$,[32] and by Geng et al. for $H_{0.8}[Ti_{1.2}Fe_{0.8}]O_4 \cdot H_2O$.[33]

The pristine sample in the dried state represents a statistically isotropic microcrystalline sample with mean tactoid diameters of 18 μm and heights of typically 1.5 μm (Figure S1 in Supporting Information). The uniquely homogeneous charge density and intracrystalline reactivity of the synthetic $Na_{0.5}$-hectorite have now allowed a systematic investigation of osmotic swelling by small-angle X-ray scattering (SAXS, Figure 2a,b and Figure S3 in Supporting Information). Consistent with the observation of Langmuir, Michot, and Miyamoto, 2D-scattering patterns of the bulk samples show a series of concentric, equidistant diffraction rings which are characteristic for lamellar lyotropic structures. The scattering patterns are highly anisotropic due to shear-alignment of the highly swollen tactoids during filling of the gels in the X-ray capillary. A high

scattering intensity is found at the equator, indicating that the layers align parallel to the surface of the vertically mounted capillary. A quantitative analysis applying model calculations reveal orientational order parameters as high as S = 0.8 (see Table S1, Supporting Information).

In Figure 2b the azimuthally averaged data are given. For higher concentrations, we observe a rational series (1:2:3:...) of $00l$-reflections indicating the formation of a lyotropic lamellar phase. Up to eight higher order reflections underline the excellent positional order of adjacent individual layers. Upon dilution, the peak positions shift to lower q-values, indicating increasing separation of the silicate layers due to progressing swelling. The interlayer distance reaches values up to 170 nm for ϕ = 0.002. The observed q^{-2}-scaling of the scattering intensity over nearly the whole scattering curve confirms the presence of thin layers with very large lateral dimensions. For the higher concentrations, where the signal-to-noise ratio is higher, it is possible to determine the first minimum of the form factor oscillations at high q (Figure 2b), which allows us to derive the thickness of the layers to d_0 = 0.85 nm. This is slightly smaller than the monolayer thickness of 0.96 nm obtained from the interlayer distance of nonhydrated $Na_{0.5}$-hectorite,[19] because small-angle X-ray scattering is sensitive to

the high homogeneous electron density of the silicate layer.

The solid lines are quantitative fits to the measured scattering intensities using a model of stacked layers where the scattered intensity is given by[39]

$$I(q) = b^2\rho P(q, d_0, D_0)[1 + \beta(q)(Z(q, d, D) - 1)G$$
$$(q, \delta)] \tag{7}$$

where b is the scattering contrast between the silicate layers and the solution, ρ the number density of the layers, q the scattering vector, $P(q)$ the form factor, d_0 the layer thickness, and D_0 the lateral layer dimension. $Z(q)$ is the lattice factor determining the interlayer distance (or lamellar long period) d as well as the peak width, which is related to the lateral size D of the ordered domains. $G(q)$ is the Debye–Waller factor, which depends on the mean deviation δ of the layers from their ideal lattice point. The term $S(q) = [1 + \beta(q)(Z(q,d,D) - 1)G(q,\delta)]$ is the structure factor, which will be discussed in a separate section. The measured scattering intensities could be well fitted to this expression to determine the layer thickness $d_0 = 0.85$ nm and the lamellae spacing, while keeping the lateral layer dimension $D_0 = 18$ μm, which was determined by electron microscopy, constant. The data are summarized in Table S1 in Supporting Information.

The λ-shaped *11/02*-band (asterisk in Figure 2b) is observed for all dilutions at the same q-values ($q \sim 1.4$ Å^{-1}), indicating that the (hk)-plane structure of the silicate layers are not influenced by the swelling in the *00l* direction of the tactoids. The lamellar distance is plotted as a function of volume fraction in Figure 2d. For high volume fractions $\phi > 0.025$, we observe a linear dependence following $d = d_0/\phi$ typical for lamellar systems[25] corroborating monolayers uniformly separated by water. As a result of strong repulsive interactions, the layers localize on a highly ordered lattice, thereby maximizing their separation. This homogeneous single gel phase of highly swollen tactoids phenomenologically resembles a Wigner crystal, which is observed for electrons in plasmas, when their repulsive interactions become much larger than their kinetic energy such that they couple, become positionally strongly correlated, and localize on lattice points with the maximum possible interelectron distance.

Transition II: Melting of Wigner Crystal (Delamination). The scaling relation given in Figure 2d shows a kink at $\phi = 0.025$. Below this volume fraction a weaker concentration dependence of the layer distance, $d \sim \phi^{-0.66}$, is observed, indicating the transition to a more disordered regime. At the same concentration, any induced shear orientation observed in 2D SAXS pattern relaxes upon cessation of shear (Figure S3). Further, the relative lattice derivations from the lattice points δ reach values over 10% (cf., Table S1). According to the Lindeman-criterium,[34] lattice melting is expected for relative displacements larger than 10%. In good agreement with all the other criteria, the structure factor (Figure 2c) confirms the melting transition, fulfilling the Hansen-Verlet criterion according to which the melting transition corresponds to a value of $S(q) = 2.85$. Larger values correspond to ordered solid, and smaller values to a molten solid. This value is crossed at a volume fraction of $\phi = 0.025$. This shows that for $d \sim \kappa^{-1}$, the Wigner lattice melts due to the screening of the long-range electrostatic interaction.

Regime III: Osmotic Swelling in the Screened Regime. When the interlayer distance becomes larger than the Debye-length $\kappa^{-1} \approx 30$ nm, a new regime characterized by $h \gg \kappa^{-1}, l_{GC}$ is reached. Here electrostatic interactions are screened beyond length scales of l_D and the osmotic pressure is given by

$$\Pi \approx \frac{8k_B T \kappa^2}{\pi l_B} e^{-d/l_D} \tag{8}$$

with a strongly screened repulsive interaction.[24] The weakening of electrostatic repulsion at transition II leads to reduced correlations of adjacent layers and melting of the Wigner crystal. As a consequence, in regime III a weaker concentration dependence of the interlayer distance, namely $d \sim \phi^{-0.66}$ (Figure 2d) is observed. For lyotropic liquid-crystalline phases of conventional molecular surfactants or block copolymers, a change in the exponential of the equation $d \sim \phi^{-\beta}$ signals a transition between different topologies: $\beta = 1$, $\beta = 1/2$, and $\beta = 1/3$ for lamellar, cylindrical (rodlike), and spherical topologies, respectively. An isotropic phase with freely rotating layers would be signaled by $\beta = 1/3$. A value of $\beta = 2/3$ would be characteristic of a bicontinuous phase.[35,36]

As such topological changes cannot occur for insoluble silicate layers, at this point the physical reason behind the $\beta = 0.66$ dependency is unclear. Michot et al. observed for size-classified nontronite also a discontinuity of the scaling from ϕ^{-1} to a variety of different slopes, depending on the size fraction.[27] The observed slopes were therefore described by a mixture of freely rotating small platelets scaling with $\phi^{-1/3}$ and a lyotropic lamellar phase of larger platelets scaling with ϕ^{-1}. Although Na$_{0.5}$-hectorite is also polydisperse, the smallest diameters seen in static laser scattering are still in the micron range.[19] Hence, the $\phi^{-1/3}$ can only be observed for $d > 1$ μm and freely rotating layers therefore can be ruled out at d-spacings where the discontinuity ($d^* \approx 34$ nm) is observed.

The change in the exponent indicates phase separation. Yet, macroscopically we do not observe phase separation in regime III at concentrations $0.025 < \phi < 0.0015$. Rather, the gels seem to undergo microphase segregation, where an ordered lamellar microphase of silicate layers (phase A) is in equilibrium with a disordered microphase of higher water content (phase B), which leads to a weaker concentration dependence of the layer distance d. In phase B, separated, but not freely rotating, layers are expected to have a folded and undulated conformation, reducing the effective lateral extension and thereby gaining conformational entropy which drives the phase separation.

Individual layers can separate from a lamellar stack or tactoid via an unbinding transition. This is known for amphiphilic lamellar systems, where lamellae unbind and detach from the top of a lamellar stack and then separate. They then fold, similar to the silicate layers, but then subsequently close to form vesicles, such that there is a concentrated ordered lamellar phase in equilibrium with a dilute vesicular phase.

Alternatively, individual layers within the lamellar stack or tactoid could translate laterally beyond the former crystal edges of the tactoid and then fold and gain conformational entropy, thereby increasing its effective diameter. The tactoid would then remain intact upon dilution, which we observe by polarized optical video microscopy (see Supporting Information). While expanding the interlayer space, the morphology of the tactoid is gradually converted from a platelet to a wormlike rod. The pristine tactoids typically have an aspect ratio of 12 (Figure S4 in Supporting Information). The aspect ratio is then inverted to 0.2 at a separation of the individual silicate layers of about 60 nm ($\phi \approx 0.01$). At these late stages of osmotic

swelling, the electrostatic repulsion between adjacent layers is increasingly screened, such that the electrosteric repulsion between adjacent tactoids becomes significant, also because with the inversion of the aspect ratio, the relative contribution of tactoid edge surface to basal surface interaction increases drastically.

Regime III is characterized by increasing widths and decreasing intensities of the Bragg peaks, indicating a reduction of the coherence length in the ordered domains, and loss of higher order reflections, corresponding to larger deviations from the lattice points. For very dilute solutions, eventually the peaks would be at very low q-values, out of the range of our SAXS-setup, with a q_{min} corresponding to $d \sim 170$ nm and $\phi > 0.0023$.

At $\phi = 0.0015$, the suspension is still viscous with no macroscopic phase separation as indicated by polarized light imaging. Experimentally, we observed no visible phase separation even over periods of several months. It may nevertheless be that at much longer periods (>1 year) and despite very slow kinetics, segregation might occur.[37,38] Below this volume fraction the two microphases start to macroscopically phase separate by gravitation as shown in Figure 3 and
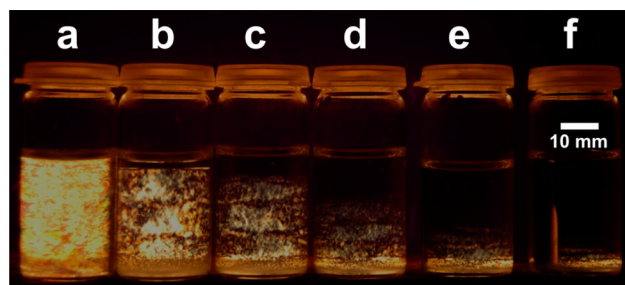

Figure 3. Macroscopic phase separation of $Na_{0.5}$-hectorite suspensions observed between crossed polarizer and analyzer. (a) $\phi = 0.0015$; (b) $\phi = 0.0008$; (c) $\phi = 0.0005$; (d) $\phi = 0.0004$; (e) $\phi = 0.0003$; (f) $\phi = 0.0002$.

Figure S5 in Supporting Information. Interestingly, for suspensions with $0.0008 < \phi < 0.0004$ (Figure 3b–d) after 2 days, phase separation results in a layered superstructure with textures with periodicities of several millimeters. At further dilution, tactoids with smaller lateral diameters will eventually start to rotate freely and be present in the supernatant phase, whose volume increases with progressing dilution (Figure 3b–f).

Eventually, upon sufficient dilution, a single dilute phase will be reached if the layer separation is on the order of the lateral dimension of the layers, e.g., if $\phi \sim d_0/D_0$. Due to the high median aspect ratio of 18000, this concentration is calculated to be extremely small, i.e., $\phi \sim 0.000056$. Indeed, a suspension close to this concentration ($\phi = 0.00009$) appears to be a single phase. It is shear-birefringent because there is still shear-induced alignment of the layers (Figure S6 in Supporting Information), but the birefringence disappears after cessation of shear.

CONCLUSIONS

We show that the delamination of charged layers requires that the layer separation exceeds the Gouy−Chapman length ($h > 2l_{GC}$) such that interactions between adjacent layers become repulsive, leading to an osmotic swelling. In the electrostatically attractive regime ($h \sim l_{GC}$), layer separation occurs by discrete

hydration steps. During initial steps of osmotic swelling, the classical double layer structure consisting of an inner and outer Helmholtz plane followed by a diffuse double layer is established. Upon further hydration, there is a regime of strong osmotic-repulsion (Gouy−Chapman regime), where the layers form a highly ordered one-dimensional Wigner crystal. When the interlayer distances reach the Debye-length, a new regime with screened osmotic repulsion is entered, accompanied by a melting of the Wigner crystal and formation of a first microscopically phase separated system. Macroscopic phase separation by gravitation does not set in until much lower concentrations ($\phi < 0.0015$). At very low concentrations ($\Phi < \sim 0.0001$), finally a homogeneous dilute phase is reached.

Our study reveals the conditions for charged layer exfoliation, provides insight into why high charge density and charge homogeneity are crucial and how the electric double layers are established, and describes the structure and property of the resulting lamellar in the limit of extreme aspect ratios, which is relevant for applications such as fillers in nanocomposite films used as a gas barrier.

ASSOCIATED CONTENT

Ⓢ Supporting Information

The Supporting Information is available free of charge on the ACS Publications website at DOI: 10.1021/acs.langmuir.6b02206.

    Supporting data (PDF)

AUTHOR INFORMATION

Present Address

∥School of Pharmacy & Biomolecular Sciences, Liverpool John Moores University, L3 3AF Liverpool, UK.

Notes

The authors declare no competing financial interest.

REFERENCES

(1) Blackmore, A. V.; Miller, R. Tactoid size and osmotic swelling in calcium montmorillonite. *Soil Sci. Soc. Am. Proc.* **1961**, 25, 169−173.

(2) Chiritescu, C.; Cahill, D. G.; Nguyen, N.; Johnson, D.; Bodapati, A.; Keblinski, P.; Zschack, P. Ultralow thermal conductivity in disordered, layered WSe_2 crystals. *Science* **2007**, 315, 351−353.

(3) Takada, K.; Sakurai, H.; Takayama-Muromachi, E.; Izumi, F.; Dilanian, R. A.; Sasaki, T. Superconductivity in two-dimensional CoO_2 layers. *Nature* **2003**, 422, 53−55.

(4) Novoselov, K. S.; Geim, A. K.; Morozov, S. V.; Jiang, D.; Zhang, Y.; Dubonos, S. V.; Grigorieva, I. V.; Firsov, A. A. Electric field effect in atomically thin carbon films. *Science* **2004**, 306, 666−669.

(5) Wu, W.; Wang, L.; Li, Y.; Zhang, F.; Lin, L.; Niu, S.; Chenet, D.; Zhang, X.; Hao, Y.; Heinz, T. F.; Hone, J.; Wang, Z. L. Piezoelectricity of single-atomic-layer MoS_2 for energy conversion and piezotronics. *Nature* **2014**, 514, 470−474.

(6) Mashtalir, O.; Naguib, M.; Mochalin, V. N.; Dall'Agnese, Y.; Heon, M.; Barsoum, M. W.; Gogotsi, Y. Intercalation and delamination of layered carbides and carbonitrides. *Nat. Commun.* **2013**, 4, 1716.

(7) Suk, J. W.; Piner, R. D.; An, J.; Ruoff, R. S. Mechanical properties of monolayer graphene oxide. *ACS Nano* **2010**, 4, 6557−6564.

(8) Kunz, D. A.; Feicht, P.; Goedrich, S.; Thurn, H.; Papastavrou, G.; Fery, A.; Breu, J. Space-resolved in-plane moduli of graphene oxide and chemically derived graphene applying a simple wrinkling procedure. *Adv. Mater.* **2013**, *25*, 1337−1341.

(9) Novoselov, K. S.; Jiang, D.; Schedin, F.; Booth, T. J.; Khotkevich, V. V.; Morozov, S. V.; Geim, A. K. Two-dimensional atomic crystals. *Proc. Natl. Acad. Sci. U. S. A.* **2005**, *102*, 10451−10453.

(10) Butz, B.; Dolle, C.; Niekiel, F.; Weber, K.; Waldmann, D.; Weber, H. B.; Meyer, B.; Spiecker, E. Dislocations in bilayer graphene. *Nature* **2014**, *505*, 533−537.

(11) Kim, S. S.; Khai, T. V.; Kulish, V.; Kim, Y. H.; Na, H. G.; Katoch, A.; Osada, M.; Wu, P.; Kim, H. W. Tunable bandgap narrowing induced by controlled molecular thickness in 2D mica nanosheets. *Chem. Mater.* **2015**, *27*, 4222−4228.

(12) Lotya, M.; Hernandez, Y.; King, P. J.; Smith, R. J.; Nicolosi, V.; Karlsson, L. S.; Blighe, F. M.; De, S.; Wang, Z. M.; McGovern, I. T.; Duesberg, G. S.; Coleman, J. N. Liquid phase production of graphene by exfoliation of graphite in surfactant/water solutions. *J. Am. Chem. Soc.* **2009**, *131*, 3611−3620.

(13) Hofmann, U. Eindimensionale quellung von graphitsäure und graphit. Die reaktionsweisen des graphits. *Colloid Polym. Sci.* **1932**, *61*, 297−304.

(14) Hofmann, U.; Kurd, E.; Diederich, W. Kristallstruktur und quellung von montmorillonit (das tonmineral der bentonittone). *Z. Kristallogr. - Cryst. Mater.* **1933**, *86*, 340−348.

(15) Lagaly, G. Characterization of clays by organic-compounds. *Clay Miner.* **1981**, *16*, 1−21.

(16) Ferrage, E.; Lanson, B.; Sakharov, B. A.; Geoffroy, N.; Jacquot, E.; Drits, V. A. Investigation of dioctahedral smectite hydration properties by modeling of X-ray diffraction profiles: Influence of layer charge and charge location. *Am. Mineral.* **2007**, *92*, 1731−1743.

(17) Mehra, O. P.; Jackson, M. L. Iron oxide removal from soils and clays by dithionite-citrate system buffered with sodium bicarbonate. *Clays Clay Miner.* **1958**, *7*, 317−327.

(18) Paineau, E.; Bihannic, I.; Baravian, C.; Philippe, A. M.; Davidson, P.; Levitz, P.; Funari, S. S.; Rochas, C.; Michot, L. J. Aqueous suspensions of natural swelling clay minerals. 1. Structure and electrostatic interactions. *Langmuir* **2011**, *27*, 5562−5573.

(19) Stöter, M.; Kunz, D. A.; Schmidt, M.; Hirsemann, D.; Kalo, H.; Putz, B.; Senker, J.; Breu, J. Nanoplatelets of sodium hectorite showing aspect ratios of ∼ 20000 and superior purity. *Langmuir* **2013**, *29*, 1280−1285.

(20) Kalo, H.; Milius, W.; Breu, J. Single crystal structure refinement of one- and two-layer hydrate of sodium-fluorohectorite. *RSC Adv.* **2012**, *2*, 8452−8459.

(21) Kalo, H.; Milius, W.; Bräu, M.; Breu, J. Synthesis and single crystal structure refinement of the one-layer hydrate of sodium brittle mica. *J. Solid State Chem.* **2013**, *198*, 57−64.

(22) Skipper, N. T.; Lock, P. A.; Titiloye, J. O.; Swenson, J.; Mirza, Z. A.; Howells, W. S.; Fernandez-Alonso, F. The structure and dynamics of 2-dimensional fluids in swelling clays. *Chem. Geol.* **2006**, *230*, 182−196.

(23) Hofmann, U.; Hausdorf, A. Kristallstruktur und innerkristalline quellung des montmorillonits. *Z. Kristallogr. - Cryst. Mater.* **1942**, *104*, 265−293.

(24) Naji, A.; Jungblut, S.; Moreira, A. G.; Netz, R. R Electrostatic interactions in strongly-coupled soft matter. *Phys. A* **2005**, *352*, 131−170.

(25) Langmuir, I. The role of attractive and repulsive forces in the formation of tactoids, thixotropic gels, protein crystals and coacervates. *J. Chem. Phys.* **1938**, *6*, 873−896.

(26) Michot, L. J.; Bihannic, I.; Maddi, S.; Funari, S. S.; Baravian, C.; Levitz, P.; Davidson, P. Liquid-crystalline aqueous clay suspensions. *Proc. Natl. Acad. Sci. U. S. A.* **2006**, *103*, 16101−16104.

(27) Michot, L. J.; Bihannic, I.; Maddi, S.; Baravian, C.; Levitz, P.; Davidson, P. Sol/gel and isotropic/nematic transitions in aqueous suspensions of natural nontronite clay. Influence of particle anisotropy. 1. Features of the I/N transition. *Langmuir* **2008**, *24*, 3127−3139.

(28) Michot, L. J.; Baravian, C.; Bihannic, I.; Maddi, S.; Moyne, C.; Duval, J. F. L.; Levitz, P.; Davidson, P. Sol-gel and isotropic/nematic transitions in aqueous suspensions of natural nontronite clay. Influence of particle anisotropy. 2. Gel structure and mechanical properties. *Langmuir* **2009**, *25*, 127−139.

(29) Paineau, E.; Antonova, K.; Baravian, C.; Bihannic, I.; Davidson, P.; Dozov, I.; Imperor-Clerc, M.; Levitz, P.; Madsen, A.; Meneau, F.; Michot, L. J. Liquid-crystalline nematic phase in aqueous suspensions of a disk-shaped natural beidellite clay. *J. Phys. Chem. B* **2009**, *113*, 15858−15869.

(30) Miyamoto, N.; Iijima, H.; Ohkubo, H.; Yamauchi, Y. Liquid crystal phases in the aqueous colloids of size-controlled fluorinated layered clay mineral nanosheets. *Chem. Commun.* **2010**, *46*, 4166−4168.

(31) Hemmen, H.; Ringdal, N. I.; De Azevedo, E. N.; Engelsberg, M.; Hansen, E. L.; Meheust, Y.; Fossum, J. O.; Knudsen, K. D. The isotropic-nematic interface in suspensions of Na-fluorohectorite synthetic clay. *Langmuir* **2009**, *25*, 12507−12515.

(32) Gabriel, J. C.; Camerel, F.; Lemaire, B. J.; Desvaux, H.; Davidson, P.; Batail, P. Swollen liquid-crystalline lamellar phase based on extended solid-like sheets. *Nature* **2001**, *413*, 504−508.

(33) Geng, F.; Ma, R.; Nakamura, A.; Akatsuka, K.; Ebina, Y.; Yamauchi, Y.; Miyamoto, N.; Tateyama, Y.; Sasaki, T. Unusually stable ∼100-fold reversible and instantaneous swelling of inorganic layered materials. *Nat. Commun.* **2013**, *4*, 1632.

(34) Lindemann, F. A. The calculation of molecular vibration frequencies. *Z. Phys.* **1910**, *11*, 609−615.

(35) Hyde, S. T. In *Handbook of Applied Surface and Colloid Chemistry*; Holmberg, K., Ed.; John Wiley & Sons: Chichester, 2001; pp 299−332.

(36) Hyde, S. T. Swelling and structure. Analysis of the topology and geometry of lamellar and sponge lyotropic mesophases. *Langmuir* **1997**, *13*, 842−851.

(37) Ruzicka, B.; Zaccarelli, E.; Zulian, L.; Angelini, R.; Sztucki, M.; Moussaid, A.; Narayanan, T.; Sciortino, F. Observation of empty liquids and equilibrium gels in a colloidal clay. *Nat. Mater.* **2011**, *10*, 56−60.

(38) Breu, J.; Seidl, W.; Stoll, A. J.; Lange, K. G.; Probst, T. U. Charge homogeneity in synthetic fluorohectorite. *Chem. Mater.* **2001**, *13*, 4213−4220.

(39) Förster, S.; Fischer, S.; Zielske, K.; Schellbach, C.; Sztucki, M.; Lindner, P.; Perlich, J. Calculation of scattering-patterns of ordered nano- and mesoscale materials. *Adv. Colloid Interface Sci.* **2011**, *163*, 53−83.